Optics Letters

SnSSe as a saturable absorber for an ultrafast laser with superior stability

Wenjun Liu,[1,2] Mengli Liu,[1] Ximei Liu,[1] Ming Lei,[1,3] and Zhiyi Wei[2,*]

[1]State Key Laboratory of Information Photonics and Optical Communications, School of Science, Beijing University of Posts and Telecommunications, Beijing 100876, China
[2]Beijing National Laboratory for Condensed Matter Physics, Institute of Physics, Chinese Academy of Sciences, Beijing 100190, China
[3]e-mail: mlei@bupt.edu.cn
*Corresponding author: zywei@iphy.ac.cn

Received 10 October 2019; revised 21 November 2019; accepted 1 December 2019; posted 5 December 2019 (Doc. ID 380183); published 10 January 2020

Compared with SnS_2 and $SnSe_2$, SnSSe shows high hole mobilities and short relaxation time, resulting in potential applications in photoelectric devices. Here SnSSe is investigated for the ultrashort pulse generation in the mode-locked fiber laser. The prepared SnSSe saturable absorber (SA) exhibits a large modulation depth of 56.75%. Because of the saturable absorption characteristic of the SnSSe SA, mode-locked pulses as short as 158.6 fs with a signal-to-noise ratio of 94 dB are obtained at 1560.9 nm. The nonlinear exploration of SnSSe offers the possibility to explore further applications of SnSSe in near-infrared regions, especially for ultrafast photonic devices and modulators.

https://doi.org/10.1364/OL.380183

The fiber laser has aroused much attention due to advantages such as compact structure and beam quality [1–4]. Up to now, the femtosecond fiber laser has not only held a critical position in the fields of material micromachining, medicine, aerospace and photo-communication [5–8], but also has greatly driven the innovation of relevant disciplines. For instance, an optical frequency comb based on an ultrafast laser can improve measurement accuracy and sensitivity [9,10]. Femtosecond optical ranging in biological systems can be used to investigate the optical properties and microstructure of research targets [11].

The rapid growth of scientific and commercial requirements has greatly promoted the development of ultrafast photon technology [12–16]. With the rise of two-dimensional (2D) materials, the research of ultrafast lasers based on saturable absorbers (SAs) has begun to usher in an upsurge of development. The materials of the SA have been extended from classical graphene [17,18], topological insulators (TI) [19,20], black phosphorus (BP) [21,22] and transition-metal dichalcogenides (TMDs) [23–28] to new materials, including MXene, bismuthene, and BP quantum dots etc. [29–31].

Meanwhile, the imperfections of existing SAs open the door for other competitors. In recent years, SnSSe has shown potential application in photoelectric devices and can be considered as a promising candidate for SA [32]. The bandgap of SnSSe is adjustable in the range of 1.08–1.25 eV, which is the optimum value of the solar spectrum [33]. In addition, it has been reported that SnSSe shows higher hole mobilities compared with SnS_2 or $SnSe_2$ [34–36]. Meanwhile, the relaxation time of SnSSe is shorter than that of SnS_2 or $SnSe_2$, which indicates that it has greater potential in the realization of ultrafast photonics [35,36].

In this Letter, a fiber laser was used for exploring the nonlinearity properties of SnSSe. The obtained SnSSe film exhibited high crystallinity and quality. In the measurement of nonlinear absorption, SnSSe exhibited a large modulation depth of 56.75% and low saturation intensity of 1.5 MW/cm.^{2} In combination with a ring laser resonator and SnSSe SA, a stable mode-locked system was demonstrated at 1560.9 nm with a bandwidth of 28.67 nm. The pulse duration obtained was 158.6 fs. To the best of our knowledge, this is the first successful application of SnSSe in fiber lasers, which reveals not only the optical nonlinearity of SnSSe, but also the enormous potential in ultrafast photonics.

With the chemical vapor transport (CVT), SnSSe is transported within a certain temperature gradient with the aid of the transfer agent to produce high-quality crystals. Then, with the help of a polymethyl methacrylate (PMMA) transfer method, PMMA-coated SnSSe is transferred to the fiber ferrule, and the PMMA is dissolved by acetone. In the experiment, SnSSe film is switched between two fiber ferrules, this integrated structure offers convenience for experiment and storage, and further provides stringent optical constraints to enhance the light-material interaction.

The surface morphology is exhibited in Fig. 1(a) using atomic force microscopy (AFM). The reference surface and film reveal a certain thickness difference, as shown in Fig. 1(b), which indicates that the thickness of the prepared SnSSe film is 109 nm. Figure 1(c) is the Raman spectrum of SnSSe, the obvious E_g and A_{1g} peaks are consistent with previous results [37]. The chemical element composition analysis of this ternary compound is investigated by X-ray photoelectron spectroscopy (XPS). In Fig. 1(d), the main peak near 54 eV is considered to be a combination of two peaks centered at 54.5 and 53.7 eV, which are related to Se $3d_{3/2}$ and Se $3d_{5/2}$, respectively. This is

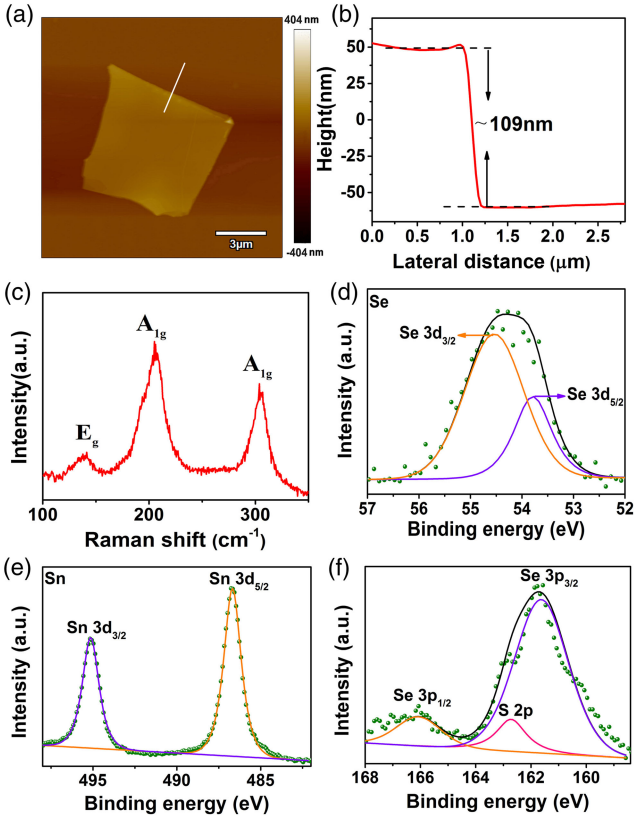

Fig. 1. Characterizations of SnSSe. (a) AFM micrographs of SnSSe; (b) height difference between SnSSe and datums; (c) Raman spectrum of SnSSe; (d) XPS spectra of Se 3d, (e) Sn 3d, and (f) S 2p, Se 3p in SnSSe.

the obvious sign that Se^{2-} exists in the sample. From Fig. 1(e), the peak separation between Sn $3d_{3/2}$ (495.1 eV) and Sn $3d_{5/2}$ (486.6 eV) is nearly 8.5 eV, which indicates the existence of Sn in IV. It is worth mentioning that the peak at 486.6 eV is also related to the S-Sn bond. From Fig. 1(f), the orbital peaks of Se $3p_{1/2}$, Se $3p_{3/2}$, and S 2p are located, respectively, at 166, 161.7, and 162.6 eV, which proves once again the existence of S element and further shows the coexistence of elements Se and S [38]. The above results demonstrate the successful preparation of SnSSe.

From the absorption curve of the SnSSe SA in Fig. 2(a), SnSSe shows a linear transmission of 75% at 1560.9 nm and presents the optical properties of SnSSe. At the same time, the bandgap of SnSSe is estimated to be 0.6 eV, which indicates that the SnSSe SA can operate in a 2 μm region. By using a two-terminal

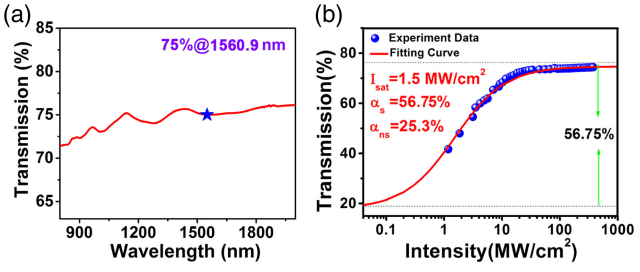

Fig. 2. (a) Linear and (b) nonlinear absorption spectrum curve of SnSSe SA.

power-dependent measurement mentioned in our previous research [26], the nonlinear absorption properties of SnSSe SA is revealed. The laser source centered at 1550 nm with 700 fs pulse duration and a 120 MHz repetition rate is used. As shown in Fig. 2(b), the absorptive capacity gap up to 56.75% at low- and high-intensity light irradiation is observed. Meanwhile, the low saturation intensity of 1.5 MW/cm^2 and small unsaturated loss of 25.35% are obtained.

An all-fiber erbium-doped fiber laser (EDFL) is established to investigate the optical nonlinearity of SnSSe, as shown in Fig 3. The driving source of the entire cavity is a 976 nm laser

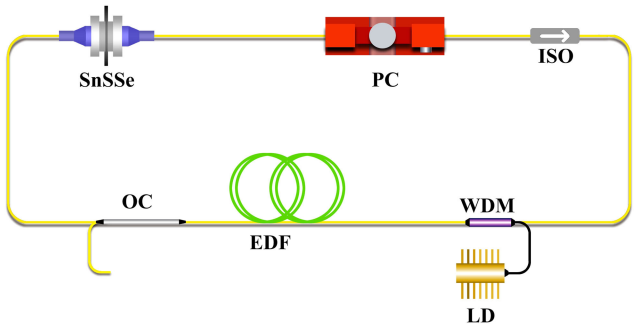

Fig. 3. Optical nonlinear verification platform for SnSSe: an all-fiber EDFL.

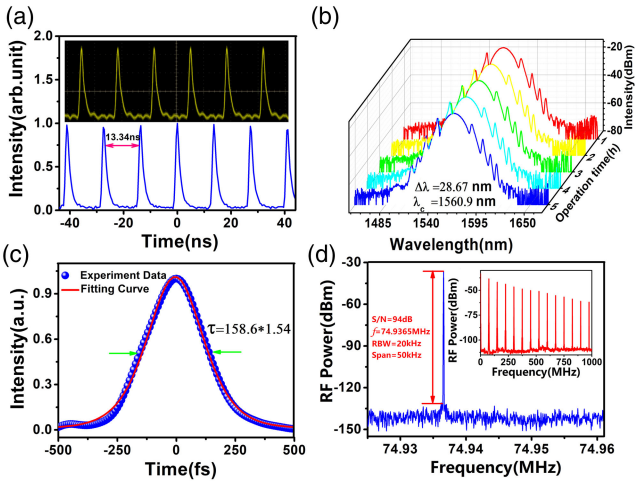

Fig. 4. (a) Pulse sequence, (b) spectrum, (c) autocorrelation trace after a sech^2 fitting, and (d) RF spectrum of the established mode-locked EDFL.

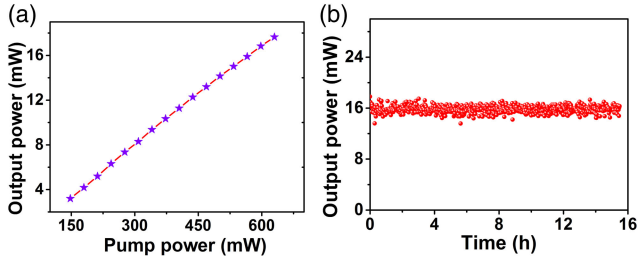

Fig. 5. (a) Functional relationship between the output power of the EDFL and the pump power; (b) output power stability monitoring up to 15 h.

Table 1. Comparison of Mode-Locked Lasers Based on Various 2D Materials

Materials	Saturation Intensity	Nonsaturated Loss	Modulation Depth	τ (fs)	Frep (MHz)	SNR (dB)	Output Power (mW)	Reference
Graphene	190 μJ/cm^2	65%	11%	88	21.15	65	1.5	[42]
BP	-	-	0.6-4.6%	272	28.2	65	0.5	[43]
Sb_2Te_3	31 MW/cm^2	43%	6%	270	34.58	70	1	[44]
MoS_2	2.02 MW/cm^2	14.74%	10.69%	960	12.99	55	-	[45]
$MoSe_2$	7.747 MW/cm^2	46.46%	22.57%	207	64.6	85	-	[16]
WS_2	157.6 MW/cm^2	45.9%	15.1%	1490	0.487	71.8	62.5	[46]
SnSSe	1.5 MW/cm^2	25.3%	56.75%	158.6	74.9365	94	17.12	This work

diode (LD), the maximum output power of which is 630 mW. Light from the LD passing through a 980/1550 nm wavelength division multiplexer (WDM), pumped a 0.4 m EDF which owns the GVD of 12 ps^2/km for the optical amplification effect of intra-cavity pulses. An isolator (ISO) is incorporated into the cavity to prevent the generation of reverse light, which ensures the unidirectional transmission of light and avoids the accidental damage of reverse light to optical devices. After a SnSSe SA is incorporated into the laser, a polarization controller (PC) is employed to control the intra-cavity polarization state and birefringence to optimize the working state of the laser. 20% of optical signals are exported through a 20/80 optical coupler for real-time optical signal characteristic detection. The measuring equipment used for optical signals is the oscilloscope (Tektronix DPO3054), radio-frequency (RF) spectrum analyzer (Agilent E4402B), and optical spectrum analyzer (Yokogawa AQ6370C).

The minimum pump power sufficient to support mode-locked output is 148 mW. With the continuous increase of power, the system maintains stable mode-locked pulse output. Figure 4 shows a summary of the performance of the mode-locked EDFL when the output power of the pump reaches a maximum of 630 mW. Figure 4(a) are the uniform mode-locked pulse trains observed on an oscilloscope, the time interval of which is 13.34 ns. Figure 4(b) is the optical spectrum of the mode-locked EDFL with symmetrical Kelly sidebands. The spectrum remains in shape during long-term monitoring with 3 dB bandwidth of 28.67 nm at a 1560.9 nm center wavelength. The autocorrelation trace after a sech^2 fitting is shown in Fig. 4(c), which demonstrates that the pulse duration is 158.6 fs. The RF spectrum has a fundamental repetition rate at 74.9 MHz in Fig. 4(d), which indicates that the mode-locked operation shows a signal-to-noise ratio (SNR) above 94 dB at the narrow resolution bandwidth (RBW) of 20 kHz. The broadband RF spectrum in the range of 1 GHz is recorded in the illustration of Fig. 4(d). The decreasing trend of the RF intensity is determined by the intrinsic property of photodetectors called the frequency response characteristic. According to previous research [39], there is no Q-switched phenomenon, and the system is stable.

In Fig. 5(a), the functional relationship between the output power of the EDFL and the pump power is revealed. The maximum output power of the mode-locked EDFL is 17.65 mW. The output power performance of a laser at the highest pump power is monitored in Fig. 5(b). During 15 h of monitoring the output power, a calculated standard deviation is 0.157 mW, which indicates the excellent stability of the system.

After SnSSe SA is removed from the cavity, no mode-locked pulse can be obtained. Our experiments show that SnSSe exhibits a SA property at 1560.9 nm (0.794 eV), which is lower than the bandgap of SnSSe in Ref. [33]. In fact, the sub-band absorption has been widely observed in TMDs. Although the internal mechanism is still uncertain, some researchers have theoretically proved that the defect state can reduce the bandgap of TMDs, and this theory has been accepted [40,41]. Therefore, as an analog of TMDs, SnSSe shows similar sub-band absorption due to the defect state.

A comparison of mode-locked lasers based on various 2D materials is shown in Table 1. According to Table 1, the prepared SnSSe SA has the maximum modulation depth of 56.75%, which is beneficial to the generation of ultrashort pulses [47]. Additionally, the nonsaturated loss is lower than that of most saturable absorption devices. Moreover, the SnSSe-based laser exhibits an SNR above 94 dB, which indicates the excellent stability of the laser. From the performance comparison of the laser, SnSSe is not inferior to the materials commonly used in the past, such as graphene, BP, and TI. Its potential in ultrashort pulse generation prompts further research for its application in ultrafast photonics.

In summary, we have demonstrated the optical nonlinearity of CVT-grown SnSSe nanosheets in the passively mode-locked EDFL. The prepared SnSSe SA shown a large modulation depth of 56.75%. After SnSSe SA is applied to the EDFL system, stable pulses with a pulse duration of 158.6 fs have been observed. The mode-locking operation at 1560.9 nm with a 28.67 nm bandwidth has shown a SNR above 94 dB, which indicated low-amplitude fluctuations and high stability of the system. To the best of our knowledge, this is the first time that the optical nonlinearity of SnSSe has been investigated in fiber lasers. The excellent performance of the EDFL system in generating ultrashort pulses with high stability demonstrates that SnSSe is a promising candidate for ultrafast photonic devices.

Funding. National Natural Science Foundation of China (11674036, 11875008, 91850209); Beijing Youth Top-notch Talent Support Program (2017000026833ZK08); State Key Laboratory of Information Photonics and Optical Communications (Beijing University of Posts and Telecommunications) (IPOC2019ZZ01); Fundamental Research Funds for the Central Universities (500419305); State Key Laboratory of Advanced Optical Communication Systems and Networks, Shanghai Jiao Tong University (2019GZKF03007); Beijing University of Posts and Telecommunications Excellent Ph.D. Students Foundation (CX2019202).

Acknowledgment. The authors thank the Beijing National Laboratory for Condensed Matter Physics for the use of equipment.

Disclosures. The authors declare that there are no conflicts of interest related to this Letter.

REFERENCES

1. B. Oktem, C. Ülgüdür, and F. Ö. Ilday, Nat. Photonics **4**, 307 (2010).
2. P. Grelu and N. Akhmediev, Nat. Photonics **6**, 84 (2012).
3. W. H. Renninger, A. Chong, and F. W. Wise, IEEE J. Sel. Top. Quantum Electron. **18**, 389 (2012).
4. M. E. Fermann and I. Hartl, Nat. Photonics **7**, 868 (2013).
5. R. R. Gattass and E. Mazur, Nat. Photonics **2**, 219 (2008).
6. J. M. White, H. E. Goodis, and C. L. Rose, Lasers Surg. Med. **11**, 455 (1991).
7. M. M. Pariona, V. Teleginski, K. dos Santos, S. Machado, A. J. Zara, N. K. Zurba, and R. Riva, Surf. Coat. Technol. **206**, 2293 (2012).
8. L. G. Luo, P. L. Chu, and H. F. Liu, IEEE Photonics Technol. Lett. **12**, 269 (2000).
9. D. J. Jones, S. A. Diddams, J. K. Ranka, A. Stentz, R. S. Windeler, J. L. Hall, and S. T. Cundiff, Science **288**, 635 (2000).
10. A. Schliesser, N. Picqué, and T. W. Hänsch, Nat. Photonics **6**, 440 (2012).
11. J. G. Fujimoto, S. De Silvestri, E. P. Ippen, C. A. Puliafito, R. Margolis, and A. Oseroff, Opt. Lett. **11**, 150 (1986).
12. M. E. Fermann, M. J. Andrejco, Y. Silberberg, and M. L. Stock, Opt. Lett. **18**, 894 (1993).
13. D. Mao, S. Zhang, Y. Wang, X. Gan, W. Zhang, T. Mei, Y. Wang, Y. Wang, H. Zeng, and J. Zhao, Opt. Express **23**, 27509 (2015).
14. W. J. Liu, M. L. Liu, S. Lin, J. C. Liu, M. Lei, H. Wu, C. Q. Dai, and Z. Y. Wei, Opt. Express **27**, 16440 (2019).
15. W. J. Liu, M. L. Liu, H. N. Han, S. B. Fang, H. Teng, M. Lei, and Z. Y. Wei, Photonics Res. **6**, C15 (2018).
16. W. J. Liu, M. L. Liu, Y. Y. OuYang, H. R. Hou, M. Lei, and Z. Y. Wei, Nanotechnology **29**, 394002 (2018).
17. Q. Bao, H. Zhang, Y. Wang, Z. Ni, Y. Yan, Z. X. Shen, K. P. Loh, and D. Y. Tang, Adv. Funct. Mater. **19**, 3077 (2009).
18. J. Bogusławski, G. Soboń, A. Przewłoka, A. Krajewska, W. Strupiński, K. M. Abramski, and J. Sotor, *Conference on Lasers and Electro-Optics Pacific Rim* (Optical Society of America, 2017), p. 1–4.
19. P. G. Yan, R. Lin, S. Ruan, A. Liu, and H. Chen, Opt. Express **23**, 154 (2015).
20. H. Zhang, C. Liu, X. Qi, X. Dai, Z. Fang, and S. Zhang, Nat. Phys. **5**, 438 (2009).
21. D. Na, K. Park, K. Park, and Y. W. Song, Nanotechnology **28**, 475207 (2017).
22. C. Q. Han, M. Y. Yao, X. X. Bai, L. Miao, F. F. Zhu, D. D. Guan, S. Wang, C. L. Gao, C. H. Liu, D. Qian, Y. Liu, and J. F. Jia, Phys. Rev. B **90**, 085101 (2014).
23. W. J. Liu, L. H. Pang, H. N. Han, M. L. Liu, M. Lei, S. B. Fang, H. Teng, and Z. Y. Wei, Opt. Express **25**, 2950 (2017).
24. W. Liu, L. Pang, H. Han, K. Bi, M. Lei, and Z. Wei, Nanoscale **9**, 5806 (2017).
25. M. L. Liu, Y. Y. Ouyang, H. R. Hou, W. J. Liu, and Z. Y. Wei, Chin. Opt. Lett. **17**, 020006 (2019).
26. M. L. Liu, Y. Y. OuYang, H. R. Hou, M. Lei, W. J. Liu, and Z. Y. Wei, Chin. Phys. B **27**, 084211 (2018).
27. W. J. Liu, M. L. Liu, B. Liu, R. G. Quhe, M. Lei, S. B. Fang, H. Teng, and Z. Y. Wei, Opt. Express **27**, 6689 (2019).
28. M. L. Liu, W. J. Liu, and Z. Y. Wei, J. Lightwave Technol. **37**, 3100 (2019).
29. Y. Xu, Z. Wang, Z. Guo, H. Huang, Q. Xiao, H. Zhang, and X. Yu, Adv. Opt. Mater. **4**, 1223 (2016).
30. X. Jiang, S. Liu, W. Liang, S. Luo, Z. He, Y. Ge, H. Wang, R. Cao, F. Zhang, Q. Wen, J. Li, Q. Bao, D. Fan, and H. Zhang, Laser Photonics Rev. **12**, 1700229 (2018).
31. L. Lu, Z. M. Liang, L. M. Wu, Y. X. Chen, Y. F. Song, S. C. Dhanabalan, J. S. Ponraj, B. Q. Dong, Y. J. Xiang, F. Xing, D. Y. Fan, and H. Zhang, Laser Photonics Rev. **12**, 1700221 (2018).
32. V. Dhanasekaran, K. Sundaram, J. Jung, and T. Mahalingam, J. Mater. Sci. Mater. **26**, 1641 (2015).
33. X. Wang, D. Chen, Z. Yang, X. Zhang, C. Wang, J. Chen, X. Zhang, and M. Xue, Adv. Mater. **28**, 8645 (2016).
34. S. Guo, X. Guo, R. Han, and Y. Deng, Phys. Chem. Chem. Phys. **21**, 24620 (2019).
35. A. Shafique, A. Samad, and Y. H. Shin, Phys. Chem. Chem. Phys. **19**, 20677 (2017).
36. Q. Bao, H. Zhang, Z. Ni, Y. Wang, L. Polavarapu, Z. Shen, Q. Xu, D. Tang, and K. P. Loh, Nano Res. **4**, 297 (2011).
37. X. Wang, C. Li, C. Liu, L. Ma, R. Li, J. Chen, and M. Xue, Electrochim. Acta **318**, 937 (2019).
38. Y. Zhang, J. Yang, Y. Zhang, C. Li, W. Huang, Q. Yan, and X. Dong, ACS Appl. Mater. Inter. **10**, 12722 (2018).
39. Y. Wang, Y. Zhao, Z. Pan, J. E. Bae, S. Y. Choi, F. Rotermund, P. Loiko, J. M. Serres, X. Mateos, H. Yu, H. Zhang, M. Mero, U. Griebner, and V. Petrov, Opt. Lett. **43**, 4268 (2018).
40. D. Mao, B. B. Du, D. X. Yang, S. L. Zhang, Y. D. Wang, W. D. Zhang, X. Y. She, H. C. Cheng, H. B. Zeng, and J. L. Zhao, Small **12**, 1489 (2016).
41. S. X. Wang, H. H. Yu, H. J. Zhang, A. Z. Wang, M. W. Zhao, Y. X. Chen, L. M. Mei, and J. Y. Wang, Adv. Mater. **26**, 3538 (2014).
42. J. Sotor, I. Pasternak, A. Krajewska, W. Strupinski, and G. Sobon, Opt. Express **23**, 27503 (2015).
43. J. Sotor, G. Sobon, W. Macherzynski, P. Paletko, and K. M. Abramski, Appl. Phys. Lett. **107**, 051108 (2015).
44. J. Sotor, G. Sobon, K. Grodecki, and K. M. Abramski, Appl. Phys. Lett. **104**, 251112 (2014).
45. M. Zhang, R. C. T. Howe, R. I. Woodward, E. J. R. Kelleher, F. Torrisi, G. H. Hu, S. V. Popov, J. R. Taylor, and T. Hasan, Nano Res. **8**, 1522 (2015).
46. P. G. Yan, H. Chen, J. D. Yin, Z. H. Xu, J. R. Li, Z. K. Jiang, W. F. Zhang, J. Z. Wang, I. L. Li, Z. P. Sun, and S. C. Ruan, Nanoscale **9**, 1871 (2017).
47. J. Jeon, J. Lee, and J. Lee, J. Opt. Soc. Am. B **32**, 31 (2015).